Energetic neutrals in the cathode sheath of argon direct-current discharges

Cite as: J. Appl. Phys. **106**, 023305 (2009); https://doi.org/10.1063/1.3160329
Submitted: 25 March 2009 . Accepted: 08 June 2009 . Published Online: 22 July 2009

Tsuyohito Ito, and Mark A. Cappelli

Energetic neutrals in the cathode sheath of argon direct-current discharges

Tsuyohito Ito[1,a)] and Mark A. Cappelli[2]
[1]*Frontier Research Base for Global Young Researchers, Frontier Research Center, Graduate School of Engineering, Osaka University, 2-1 Yamadaoka, Suita, Osaka 565-0871, Japan*
[2]*Mechanical Engineering Department, Stanford University, Stanford, California 94305-3032, USA*

(Received 25 March 2009; accepted 8 June 2009; published online 22 July 2009)

We recently reported on the direct measurements of the energy distribution of energetic neutrals incident onto the cathode of an argon dc glow discharge [T. Ito and M. A. Cappelli, Appl. Phys. Lett. **90**, 101503 (2007)]. In this paper, we provide a more extensive report of the experimental data, as well as direct comparisons to Monte Carlo simulations in which neutral-neutral and ion-neutral collision processes are modeled with differential scattering cross sections. The experimental results, which are limited to relatively small forward angle sampling in our present configuration, are found to be in excellent agreement with Monte Carlo simulations. The simulations reveal that high energy neutrals are striking the cathode with a wide range of angles, while ions are more anisotropic. Therefore, it is difficult to predict the neutral energy distribution with commonly used simple analytical models that do not consider scattering of neutrals within the sheath. We propose the use of an extended analytical model in this paper, which seems to provide reasonable energy distributions over the range of discharge voltage studied. © *2009 American Institute of Physics*. [DOI: 10.1063/1.3160329]

I. INTRODUCTION

Energetic neutrals originally formed by collisions with accelerated ions in the sheaths of direct-current (dc) discharges contribute to secondary electron emission, electrode erosion, and discharge gas heating. While many measurements have been made of the ion energy distribution in dc sheaths and good agreement is seen with analytical predictions,[1–3] with the exception of a prior study by Armour *et al.*,[4] there seemed to be no direct measurements of the energy distribution of neutrals at the cathode in dc discharges prior to our previous letter.[5] This is despite the availability of various analytical models[6–9] and computational studies.[9–11] The experiments of Armour *et al.*[4] employed an electron impact source to ionize neutrals for filtering the energy in a quadrupole spectrometer and subsequently detecting them as ions. The observed distributions are affected by this ionization process, in part due to the nonconstant probability of ionization, as pointed out by a study of the neutral energy distribution at the powered electrode of a radio-frequency argon discharge.[12] Our paper presents direct time-of-flight (TOF) measurements of high-energy neutrals impinging on the cathode in argon dc glow discharges, as also reported in the previous letter.[5] The variation in the energy distribution with discharge voltage is characterized and compared to revised Monte Carlo (MC) simulations, in which neutral-neutral and ion-neutral collision processes are accounted for using differential scattering cross sections. A rather novel analytical model is also proposed in this report, validated in part by comparison to the MC simulations, as well as the previously reported simpler analytical models.[6–8]

II. EXPERIMENTS

The measurements were made of argon neutrals drifting parallel to the electric field direction, i.e., perpendicular to the cathode of a dc discharge cell, as shown in Fig. 1. The TOF apparatus is similar to that used to characterize energetic neutrals generated in fusion edge plasmas and from sputtering targets.[13,14] The abnormal dc glow discharges are generated in pure argon at a pressure of 0.5 Torr with a 6×10^{-2} m diameter copper cathode, a stainless-steel anode, and an electrode separation of 5×10^{-2} m. Figure 2 shows the typical current-voltage characteristics of the discharge indicating that the discharge is in the abnormal glow regime. Also shown in Fig. 2 are the conditions used in MC simulations as described below. Energetic neutrals formed near the cathode are sampled through a 1×10^{-4} m diameter orifice ($\sim5\times10^{-5}$ m thick cathode foil). The sampled beam is interrupted by a high-speed (20 000 rpm) chopper, placed 3×10^{-2} m downstream of the orifice, which contains a single 3×10^{-4} m wide slit (S_1 in Fig. 1) on its blade, 4×10^{-2} m from the rotational axis. The drifting neutral stream impinges onto a 17 stage electron multiplier containing Cu–Be dynodes, located 0.9 m downstream of the chopper. A second (3×10^{-3} m wide) slit (S_2) is placed in front of the electron multiplier for improving temporal response. A positively bi-

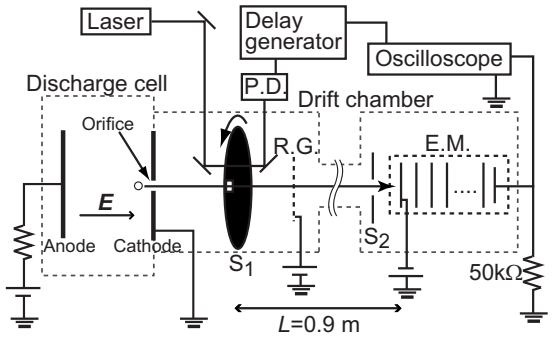

FIG. 1. Schematic of the experimental setup for measuring neutral energy distribution: anode, cathode, slit 1 and 2 (S_1 and S_2), positively biased ion retarding grid (R.G.), photo diode (P.D.), and electron multiplier (E.M.).

a)Electronic mail: tsuyohito@wakate.frc.eng.osaka-u.ac.jp.

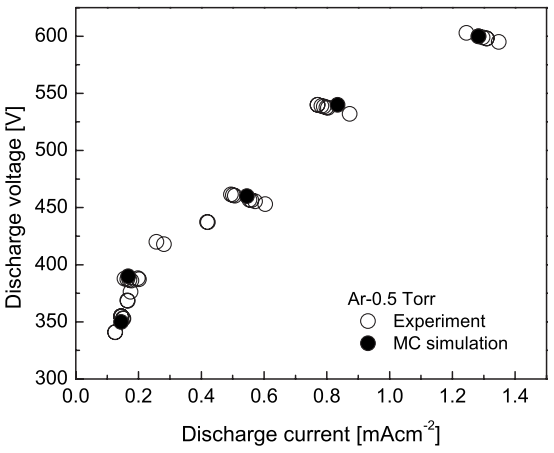

FIG. 2. Discharge current-voltage characteristics.

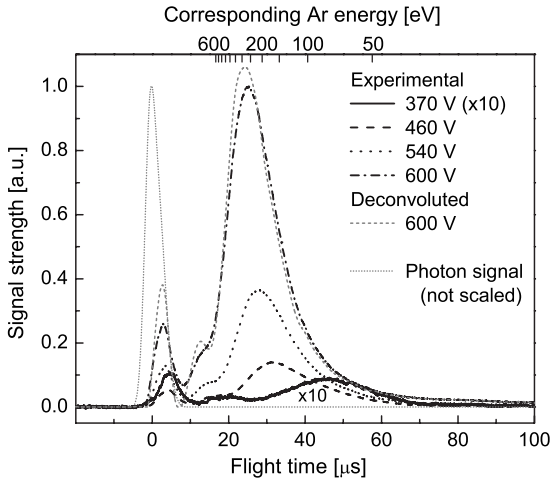

FIG. 3. Observed time of flight spectra for a range of discharge voltage, deconvolved spectrum for 600 V, and the photon signal used for the deconvolution process. TOF signals are normalized by the maximum value of the spectra for the 600 V discharge case.

ased grid (R.G. in Fig. 1) is placed just downstream of the discharge cathode and the chopper to serve as an ion filter, allowing only neutrals to pass into the drift chamber and migrate toward the electron multiplier. It is verified that the threshold grid voltage required to filter out all of the ions is close to the discharge voltage, as expected. For the results described here, the ion filter voltage is set to at least 500 V higher than the discharge voltage. The arrival of the negatively charged species, such as electrons and negative ions, to the cathode should be negligibly small because of the strong electric field repelling those species from the cathode. Furthermore, those negatively charged species cannot reach the detector, which is highly biased to a negative voltage of about -5 kV. The solid angle collected by the spectrometer, as limited by the slit in front of the detector, is $\sim 7.5 \times 10^{-5}$ sr.

The drift chamber is pumped by two turbo molecular pumps maintaining a pressure of less than $\sim 10^{-6}$ Torr during the measurements. At this pressure, the argon mean free path is longer than 50 m, so that the effects of collisions between neutrals in the drift chamber are negligible. A He–Ne laser modulated by the same chopper is used as a timing reference for triggering the oscilloscope, on which the TOF traces are recorded and averaged. The zero-drift time is determined by the signal corresponding to detected photons from the discharge observed with reverse polarity (so that the orifice is now on the anode and there is little or no detected energetic neutral signal). The photon signal has a 5 μs rise time with a full width at half maximum of 5 μs, as shown in Fig. 3 below. This signal serves as an indication of the instrument broadening and is used to deconvolve the TOF spectra.

III. MONTE CARLO SIMULATIONS

The MC simulations use a sheath thickness and potential distribution determined from the collisional form of Child's law,[15] assuming a constant charge exchange cross section (Q_{ch}) of 4×10^{-19} m^2. The estimated sheath thickness was from 2.2 mm (600 V) to 3.8 mm (350 V) and the ratio of a mean free path of ion to the sheath thickness was approximately 20 (14 for 600 V and 24.5 for 350 V). Measurements of the ion energy distribution from similar discharges suggest that the charge exchange cross sections should be in the range of $3.7–5.3 \times 10^{-19}$ m^2 (Refs. 1–3) and one can also find reference to a range of values, i.e., from 4×10^{-19} to 7.2×10^{-19} m^2 in uniform electric field experiments.[16] One can also find energy dependent cross sections accounting for reduced backscattering with increasing energy, i.e., from $\sim 5 \times 10^{-19}$ m^2 at 1 eV to $\sim 3 \times 10^{-19}$ m^2 at 1000 eV, both in theoretical and experimental studies.[17–19] In our MC simulations, ions are introduced at the sheath edge with random velocities, sampling these velocities from a Maxwellian distribution at the presumed gas temperature of 300 K. The reason for using this boundary condition for the ion velocities, instead of the usual Bohm velocity, is that this condition is consistent with the zero electric field that we impose at the sheath edge and in the boundary conditions used in simple analytical models.[1–3,6–8] We also impose this condition in our extended analytical model presented below. In this way, we are able to more directly compare our MC simulation results to these analytical models. It is also noteworthy that employing the Bohm velocity corresponding to an electron temperature of several eV has only a minor effect on the overall results. In the treatment of particle collisions, both elastic neutral-neutral and ion-neutral collisions are accounted for using the energy-dependent differential cross sections reported by Phelps *et al.*[20,21] Neutral particle velocities are neglected in evaluating the collision probabilities for ions (but are accounted for in determining the postcollision velocities). For neutral-neutral collisions, only particles with energy greater than 5 eV are considered, and their collision partner's velocities are also not considered in evaluating collision probabilities.

Direct comparison is made of the simulated neutral energy distributions to the TOF measurements by considering only those simulated neutral particles impinging on the cathode within the solid angle limited by the detector used in the experiments. These comparisons are carried out for the discharge conditions (voltage and current) shown as solid circles in Fig. 2. These conditions are also used in evaluating the appropriateness of analytical models, described in more

detail below. In the MC simulations presented here, neutrals with energy of less than 5 eV are not followed, resulting in considerable savings in computational expense.

IV. ANALYTICAL MODEL

There are several analytical models reported for the neutral energy distributions impinging onto the cathode surface in dc glow discharges. However the models, largely based on the model proposed by Abril *et al.*[6,7] and Mason and Allott,[8] do not consider energy dispersion caused by neutral-neutral collisions and the concomitant scattering into off-axis angles. The analytical model proposed by Hagelaar *et al.*,[9] which establishes upper and lower limits for the neutral energy through a rate equation based description using a local field approximation, does consider neutral-neutral collisions. However the use of a local field model may not be suitable for computing energy distribution in the cathode fall (except perhaps for the very low energy portion of the ion energy distributions) where the electric field variation is significant.

Here, we propose a relatively simple model that considers neutral-neutral collisions as well as potential variations in the cathode fall in establishing the neutral energy distribution. Only the forward fluxes (ion's and neutral's) are considered. A constant cross section (4×10^{-19} m^2) is employed for ion-neutral charge exchange collisions and an energy-dependent (elastic and isotropic) cross section[20] is employed for neutral-neutral collisions. Constant ion-neutral charge exchange cross sections are widely used in such models, as the resulting ion energy distribution is greatly simplified,[1–3] and yet is still in reasonable agreement with experiments. Neutral-neutral collisions are assumed to be isotropic elastic collisions in our analytical model.

The analytical model developed here uses the same potential distribution, $V(x)$, as was used in the MC simulations described above. Its variation with distance from the sheath edge x is given by

$$V(x) = V_c\left\{1-\left(\frac{x}{S}\right)^{5/3}\right\}, \tag{1}$$

where V_c is the cathode voltage and S is the sheath thickness, estimated by using the collisional form of the Child–Langumuir law. This potential distribution is in good agreement with particle-in-cell simulations for similar dc discharges.[2] Similar to the analyses in previous papers,[1–3] which assume that the dominant process for energy loss of ions is a charge exchange collision, we can derive the ion energy distributions f as a function of energy, ε (in volts), angle from the electric field direction θ, and the distance from the sheath edge

$$f(\varepsilon,\theta,x) = \begin{cases} \frac{3}{5}\frac{n\sigma_{ch}S}{V_c}\left\{\frac{V_c-V(x)-\varepsilon}{V_c}\right\}^{-2/5} \exp\left[-n\sigma S\left\{\left(\frac{V_c-V(x)}{V_c}\right)^{3/5}-\left(\frac{V_c-V(x)-\varepsilon}{V_c}\right)^{3/5}\right\}\right] + \exp(-n\sigma x)\,\delta(\varepsilon-(V_c-V(x))) \\ \quad (\varepsilon \le V_c - V(x) \quad \text{and} \quad \theta = 0) \\ 0 \quad (\theta \ne 0) \end{cases} \tag{2}$$

Here, n is the neutral particle density, σ_{ch} is the cross section for the charge exchange collision, and δ is Dirac's delta function. In deriving this, we assume that the ion's velocity is oriented along the direction of the electric field (which is perpendicular to the cathode), because in this analytical treatment, we assume that the charge exchange collision does not result in angular scattering.

The origins of fast neutrals are charge exchange collisions and scattering collisions between faster neutrals. Fast neutrals will also lose energy through scattering collisions with background neutrals. The resulting equation governing the evolution of the energetic cathode-directed neutral particle energy and angular distribution, $g(\varepsilon,\theta,x)$, can be expressed as

$$\frac{d}{dx}g(\varepsilon,\theta,x)d\varepsilon d\theta = f(\varepsilon,\theta,x)\frac{n\sigma_{ch}}{\cos\theta}d\varepsilon d\theta + \int_{\varepsilon}^{V_c}\int_{0}^{\pi/2} g(\varepsilon_a,\theta_a,x)\frac{nQ_{sc}(\varepsilon_a)}{\cos\theta_a}P(\varepsilon_a,\varepsilon)R(\theta_a,\theta)d\theta_a d\varepsilon_a - g(\varepsilon,\theta,x)\frac{nQ_{sc}(\varepsilon)}{\cos\theta}d\varepsilon d\theta. \tag{3}$$

In this expression, we are neglecting the second-order effect of backward directed neutrals, which, through subsequent collisions, can become cathode-directed neutrals. Also, the distribution $g(\varepsilon,\theta,x)$ describes just those neutrals originating from interactions with energetic ions or subsequent collisions with energetic neutrals and does not include the energy distribution of the otherwise thermalized background gas. In Eq. (3), $Q_{sc}(\varepsilon)$ is the energy-dependent neutral scattering cross section, the first term on the right side represents the charge exchange collision rate, and the third term is the neutral scattering loss rate. The second term on the right side of Eq. (3) represents the neutral scattering production rate, which contains the probability for scattering into a particular energy class $[P(\varepsilon_a,\varepsilon)]$, and into a particular angle $[R(\theta_a,\theta)]$, as described below.

For isotropic elastic collisions (in the center of mass

frame) between like particles, the probability, $P(\varepsilon_a,\varepsilon)$, that a particle with energy ε_a creates a particle with energy ε is given by

$$P(\varepsilon_a,\varepsilon) = 2d\varepsilon/\varepsilon_a. \tag{4}$$

The factor of 2 appears here because the collision creates two energetic neutrals which are indistinguishable.

In determining $R(\theta_a,\theta)$, we use the following relationship between the scattering angles in the laboratory frame:

$$\cos\theta = \cos\theta_a \cos\alpha - \sin\theta_a \sin\alpha \cos\beta. \tag{5}$$

Here, θ and θ_a represent the post- and precollision angles that either of the colliding particles makes relative to the electric field direction, respectively, α is the angle between the pre- and postcollision velocity, and β is the polar angle defined by the postcollision velocity relative to the direction aligned with the precollision velocity. For isotropic scattering between like particles, the particle energies are related to the angle α by

$$\varepsilon = \tfrac{1}{2}(\cos 2\alpha + 1)\varepsilon_a = \varepsilon_a \cos^2\alpha. \tag{6}$$

Using Eq. (5) together with Eq. (6), we find that the probability that some initial particle with angle θ_a collides with another particle to produce a particle with angle θ, is described by

$$R(\theta_a,\theta) = \begin{cases} \dfrac{1}{\pi}\left|\dfrac{d\beta}{d\theta}\right| d\theta = \dfrac{\sin\theta}{\pi\sqrt{\sin^2\theta_a \sin^2\alpha - (\cos\theta_a\cos\alpha - \cos\theta)^2}}d\theta & \\ = \dfrac{\sin\theta}{\pi\sqrt{\left(1-\dfrac{\varepsilon}{\varepsilon_a}\right)\sin^2\theta_a - \left(\sqrt{\dfrac{\varepsilon}{\varepsilon_a}}\cos\theta_a - \cos\theta\right)^2}}d\theta & \left(\left|\dfrac{\cos\theta_a\cos\alpha - \cos\theta}{\sin\theta_a\sin\alpha}\right| \leqslant 1\right) \\ 0 & \left(\left|\dfrac{\cos\theta_a\cos\alpha - \cos\theta}{\sin\theta_a\sin\alpha}\right| > 1\right) \end{cases} . \tag{7}$$

Equation (3), together with Eqs. (2), (4), and (7), can be solved using the Euler method with the boundary condition $g(\varepsilon,\theta,0)=0$.

If we neglect the second and third terms on the right hand side of Eq. (3), then our result reduces to the analytical model of Abril *et al.*[6,7] Neglecting only the second term and retaining the third term but with the simplification that a constant (energy independent) stopping cross section (stopping factor) is used instead of Q_{sc}, reduces our model to the analytical model proposed by Mason and Allott.[8] We compare our results to these two limiting cases, as well as to our MC simulations, in the section below.

V. RESULTS AND DISCUSSION

A. Experimental results

Representative experimental (uncorrected) TOF spectra for varying discharge voltage are shown in Fig. 3. The increases in signal intensity and a shift in peak position to shorter drift times with increasing voltage are apparent. The corresponding energy spectra are obtained following deconvolution and correction for the energy dependence of the secondary electron emission of neutral argon on Cu–Be, i.e., 1.5×10^{-3} at 50 eV, 2.5×10^{-2} at 200 eV, and 1.5×10^{-1} at 400 eV.[22] It is noteworthy that the secondary electron emission can depend on surface conditions, as pointed out by Phelps *et al.*[23] We have not pretreated or cleaned the Cu–Be dynode for these studies and therefore employ the secondary emission coefficient for untreated (native) Cu–Be surfaces, as reported in Ref. 22. The secondary electron emission also depends on energy and the uncertainty in this energy dependence is the main source of error in the analysis. A compilation of the secondary electron emission of argon atoms incident on a range of untreated materials[23] shows that the coefficients (absolute and energy dependence) all fall within a factor of 2 of each other in the high energy region (e.g., >100 eV). In this regime, we thus believe that the coefficients used in our study are accurate to within a factor of 2. In the low energy region (<100 eV), scatter in the data described in Ref. 23 precludes a certainty in the energy dependence of our extracted distributions to better than a factor of ~3. Also shown in Fig. 3 are the photon signal and the 600 V case deconvolved for instrument broadening using this photon signal. As seen in the TOF spectra of Fig. 3, there are weak peaks between 0–5 and 10–20 μs, the origin of which is attributed to hydrogen and oxygen contamination, perhaps as a result of sputtering of surfaces within the drift section of the spectrometer. These peaks were not sensitive to Ar flow rate and there was only weak optical emission associated with hydrogen, and no emission due to oxygen, from the discharge itself, reducing the likelihood that this contamination originates in the discharge. These interferences precluded energy measurements beyond an energy of approximately 200 eV for the lowest discharge voltage case shown (370 V) and about 500 eV for the highest discharge voltage (600 V) shown. Operation of the discharge on helium confirmed that there is no contamination from heavier species that might overlap with the argon signal at lower energy.

Figure 4 shows the converted neutral energy spectra (thick lines). The variation in neutral energy distribution with

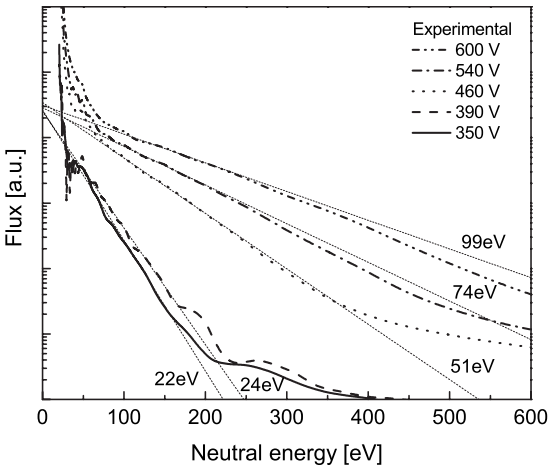

FIG. 4. Measured neutral argon energy distribution. The thin dotted lines are superimposed Maxwellian distributions at the indicated temperatures for comparison. Note that high energy regions (e.g., $>\sim 350$ eV for 460 V) may be affected by contamination from light elements.

discharge voltage is apparent, with a higher discharge voltage resulting in a more populated high energy tail. The near-linear variation in the logarithmic energy distribution is indicative of an energetic tail that is close to Maxwellian. Thin dotted lines in the figure represent this Maxwellian distribution at the labeled temperature for comparison. It is noteworthy, as mentioned above, that high energies might be affected by contamination from light elements such as H and O. The very low energy range (e.g., <50 eV) is less accurate because of the low signal as a result of low secondary electron emission yields and because of the larger uncertainty in the secondary electron emission coefficient employed in the data reduction, as mentioned above. It should be noted that the experimental reproducibility was quite good. The slope of the near-Maxwellian tail between 100 and 150 eV was determined for multiple scans at the same discharge voltage and the results are plotted for varying discharge voltage in Fig. 5. The corresponding Maxwellian temperature (which decreases with increasing slope) is clearly seen to rise with increasing discharge voltage. At any given voltage, the slope of this tail is reproducible to within 10%.

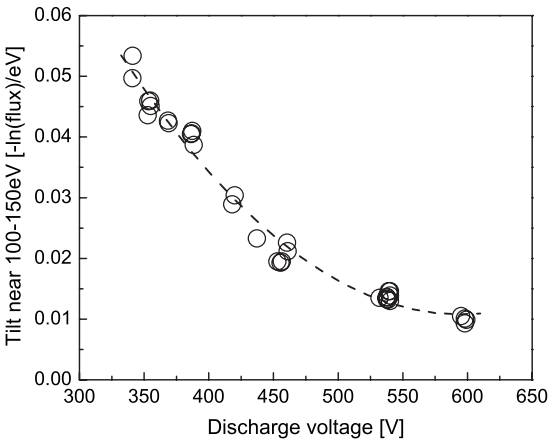

FIG. 5. Slope of the distribution functions near 100–150 eV as seen in the measurements.

B. Results of MC simulations and comparison to experiments

Results of the MC simulations are given in Fig. 6. This figure depicts particle distributions (number of particles per unit solid angle per second) at the cathode plane as functions of energy and scattering angle (0° corresponds to the direction aligned with the electric field). We can see that ions (left panels) are primarily scattered into a very narrow angle, since small-scattering angle collisions (generally charge exchange collisions) are dominant[21] and ions are accelerated by the electric field. In contrast, neutrals (right panels) are scattered into a wider range of angles. The broadening in the neutral distributions arises in part because the high energy neutrals generated by ion-neutral collisions are no longer accelerated and can subsequently collide with other neutrals.

The color maps of Fig. 6 have the same color scale for both the neutrals and ion particle flux. It is apparent then that the energy flux delivered by neutrals is much higher than that of the ions over most incident particle angles (with the exception perhaps of angles less than 5°) for all conditions investigated. This confirms that for some applications of collisional dc discharges, the role played by neutral particles in energy deposition must be considered. For example, the cathode erosion resulting from impinging particles considering the direct ion flux alone may be underestimated. Also, such a wide angular distribution seen in neutral energy might affect the design of masking processes in the plasma-assisted manufacturing of nanostructured materials.

Figure 7 compares the measured neutral energy distributions to those predicted by the MC simulations. In this comparison to the TOF data, we consider only the particles impinging on the cathode within the solid angle limited by the detector used in the experiments. We see that very good agreement is obtained between the measured and predicted distributions. It is noteworthy that the relative intensity for different discharge voltages (for either the predicted or measured distributions) is not adjusted once the experimental distribution for the 350 V case is scaled to the level of that simulated. We find that if we adjust the scale so that the 350 V experiments match the simulations, then the 600 V case is found to slightly overpredict the measured flux and this difference might be attributable to the uncertainty in estimating the experimental current density at the center of the discharge (based on an assumed discharge uniformity).

C. Analytical model predictions and comparison to MC simulations

Before presenting the predictions of our analytical model for the neutral energy distributions, we compare in Fig. 8, the ion energy distributions predicted by the simple analytical model of Davis and Vanderslice,[1] modified slightly by Budtz-Jørgensen *et al.*[2] to our MC simulations. Since the ion velocities determined from the MC simulation are found to be nearly parallel to the electric field (as seen from Fig. 6), it is not surprising that the ion energy distributions determined using the models of Refs. 1 and 2, in which no scattering is considered, results in good agreement with the MC simulations, except perhaps in the very high-energy tail. The differ-

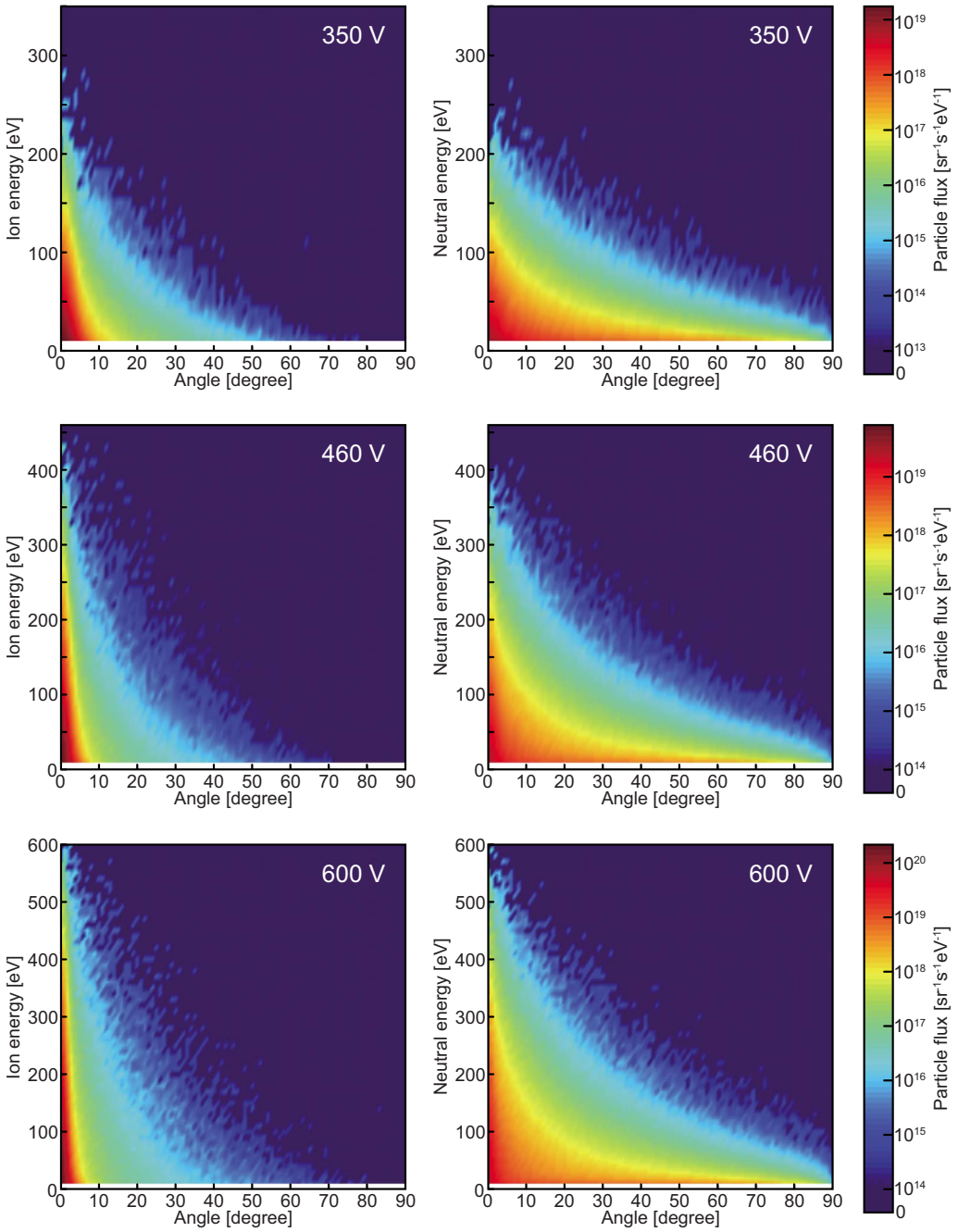

FIG. 6. (Color online) Particles flux map at the cathode as functions of scattering angle and particle energy by MC simulations: ions (left panels) and neutrals (right panels). Note that these maps are generated using binning parameters of 10 eV for energy and 1° for scattering angle.

ence at high-energy is attributed to the difference in the cross sections used; a constant cross section is assumed in the analytical models,[1,2] whereas a more realistic differential scattering cross section accounting for reduced backscattering with increasing energy[21] is employed in the MC simulations.

Figure 9 compares the neutral energy distributions predicted by our simple analytical model, which includes particle scattering [Eq. (3)], to those predicted by the MC simulations. Also for comparison, Figs. 10 and 11 include the analytical models proposed by Abril *et al.*,[6,7] and by Mason and Allott,[8] respectively. Because these previously reported models do not account for the possibility of scattering into a range of angles, Figs. 9–11 compares the energy distributions to those determined by the MC simulations for neutrals scattered into all possible angles (the angle dependence predicted by our proposed model is presented in Fig. 12). The model of Mason and Allott[8] requires specifying the so-called particle "stopping cross section", which we find to be $0.2 \times \sigma_{ch}$ for best agreement with the MC simulations. An inspection of these three figures reveals that there is little difference between the three analytical models at high energy, since the high energy particles are generated nearer to the cathode surface and, as a result, do not have time to collide before crossing the cathode plane. Greater differences between the analytical model predictions are seen in the mid-low energy region. Since the analytical model of Abril *et al.* (Fig. 10) does not include collisions between neutrals, the flux of moderate-energy particles, which should experience colli-

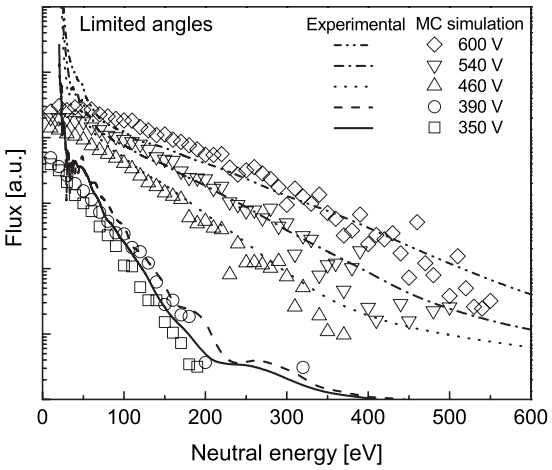

FIG. 7. Measured (thick lines) and MC simulations (symbols) of the neutral argon energy distribution. Both the measured and simulated distributions are for neutral atoms sampled over the limited detection angle of the experiment.

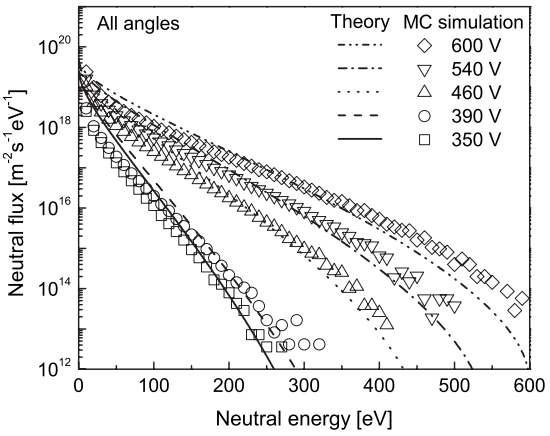

FIG. 10. Analytical models (lines) proposed by Abril *et al.* (Refs. 6 and 7) and MC simulations (symbols) of the neutral energy distribution.

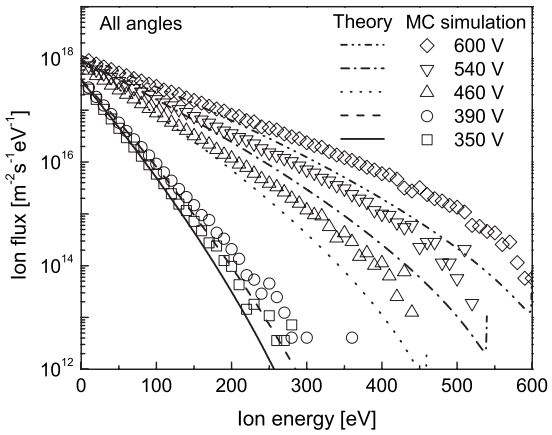

FIG. 8. Analytical models (lines) and MC simulations (symbols) of the ion energy distribution.

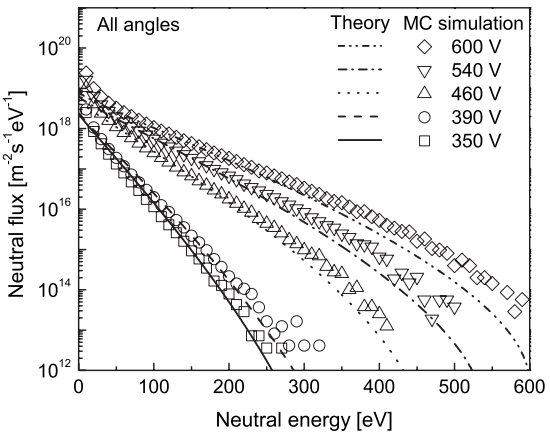

FIG. 11. Analytical models (lines) proposed by Mason and Allott (Ref. 8) and MC simulations (symbols) of the neutral energy distribution. The stopping cross section used in the analytical model was $0.2 \times \sigma_{ch}$.

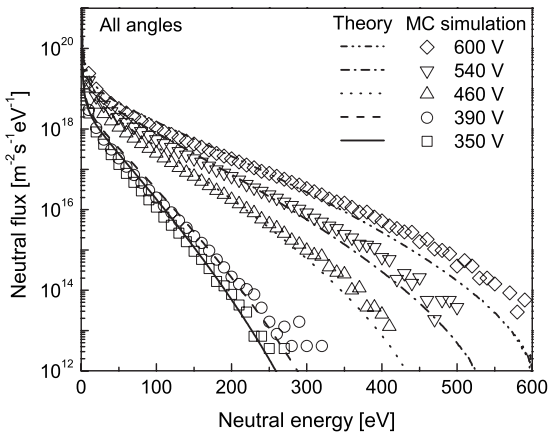

FIG. 9. Analytical models (lines) proposed in this paper and MC simulations (symbols) of the neutral energy distribution.

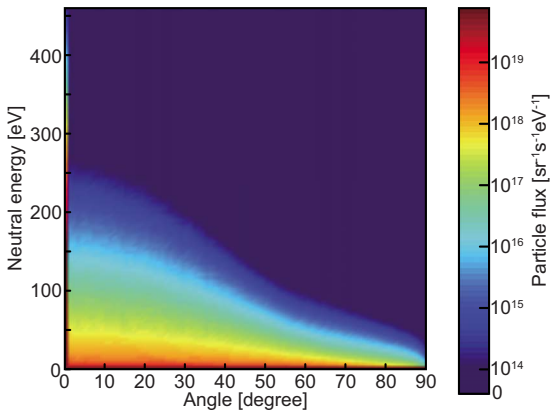

FIG. 12. (Color online) Neutral flux map as a function of scattering angle and energy by the analytical model proposed, 460 V. Note that the map is generated using binning parameters of 1 eV for energy and 1° for scattering angle.

sions before striking the cathode, is overestimated. The model of Mason and Allott (Fig. 11) fails to capture the distribution at very low energy (e.g., <80 eV for the 600 V case), where the effect of neutrals generated by neutral-neutral collisions is important. It is noteworthy again that the previously reported analytical models do not include any angle dependent distributions in the energy for the neutrals.

Although some differences between our proposed analytical model and the MC simulations are apparent, particularly the slight underprediction in the distribution at high energy, the model, which includes neutral collisional effects, seems to do a better job than those of Refs. 6–8, especially in the shape in the low-middle energy regions. We attribute this improved agreement to the introduction of the possibility of scattering into a range of angles. As stated earlier, the models of Refs. 6–8 do not include this scattering, despite its importance, as apparent in the analytical model predictions of a relatively large neutral flux at large scattering angles, as shown in Fig. 12. Despite the good agreement between the proposed analytical model and the MC simulations for the neutral energy distribution, there is good agreement only at the wide scattering angle in the angle distributions. We attribute the poor agreement in the narrow scattering angle ($<\sim 20°$) to the use of simplified scattering models, such as isotropic scattering for the neutral-neutral collisions (resulting in low probability of narrow-angle scattering) and zero-angle scattering for the ion-neutral collisions. The analytical model may therefore be improved by using differential scattering cross sections for those collisions. However, such improvements come at the expense of computational time and we believe that any further computational expense is better invested in carrying out full MC simulations.

VI. SUMMARY

In this paper, we compare the results of direct measurements of the energy distribution of neutral particles incident onto the cathode of a dc glow discharge to MC simulations (which employ differential scattering cross sections) and also compare a relatively simple analytical model to the MC simulations. The measurements are found to be in good agreement with the MC simulations, although the comparison is made only for a forward scattering angle of the neutrals that is limited to the corresponding solid angle of detection by the TOF spectrometer. The simple analytical model proposed assumes the use of a constant charge exchange cross section and isotropic scattering between neutrals. Despite this simplification, which makes its use relatively straightforward, it leads to very reasonable agreement with the results of the MC simulations. The comparison between the previously reported analytical models of Abril *et al.*[6,7] and Mason and Allott[8] seems to indicate that the scattering between neutrals, which is neglected entirely by Abril *et al.* and simplified by Mason and Allott, might be important.

It appears, from our MC simulations, that in some cases, the energy flux delivered to the cathode by neutrals can be higher than that delivered by ions in the collisional sheath. It is also noteworthy that a wide angle of scattering is seen in the neutral particle distributions. Although high energy neutrals can be found within a narrow scattering angle, the energy flux that is predicted to be at wider angles may be too large to be neglected for the purpose of estimating energy transfer to the cathode.

ACKNOWLEDGMENTS

We would like to thank Professor A. V. Phelps (JILA) for providing us with unpublished neutral-neutral differential cross sections for argon and for very helpful comments and stimulating discussions. We would also like to thank W. S. Crawford for technical assistance in carrying out the experiments. T.I. would like to thank Professor Hamaguchi (Osaka University) for his encouragement. This research was initially funded in part through the NSF/DOE Basic Plasma Sciences Initiative Grant No. DE-FG02–06ER-54897, and continued funding was provided by the Frontier Research Base for Global Young Researchers, Osaka University, through the program Promotion of Environmental Improvement to Enhance Young Researchers' Independence, the Special Coordination Funds for Promoting Science and Technology, Japan Ministry of Education, Culture, Sports, Science and Technology. Support for T.I. during his stay at Stanford was provided by the JSPS Postdoctoral Fellowships for Research Abroad Program.

[1] W. D. Davis and T. A. Vanderslice, Phys. Rev. **131**, 219 (1963).
[2] C. V. Budtz-Jørgensen, J. Bøttiger, and P. Kringhøj, Vacuum **56**, 9 (2000).
[3] T. Ito and M. A. Cappelli, Phys. Rev. E **73**, 046401 (2006).
[4] D. G. Armour, H. Valisadeh, F. A. H. Soliman, and G. Carter, Vacuum **34**, 295 (1984).
[5] T. Ito and M. A. Cappelli, Appl. Phys. Lett. **90**, 101503 (2007).
[6] I. Abril, A. Gras-Marti, and J. A. Vallés-Abarca, Phys. Rev. A **28**, 3677 (1983).
[7] I. Abril, A. Gras-Marti, and J. A. Vallés-Abarca, J. Phys. D **17**, 1841 (1984).
[8] R. S. Mason and R. M. Allott, J. Phys. D **27**, 2372 (1994).
[9] G. J. M. Hagelaar, G. M. W. Kroesen, and M. H. Klein, J. Appl. Phys. **88**, 2240 (2000).
[10] V. V. Serikov and K. Nanbu, J. Appl. Phys. **82**, 5948 (1997).
[11] I. Revel, L. C. Pitchford, and J. P. Boeuf, J. Appl. Phys. **88**, 2234 (2000).
[12] J. Janes and K. Börnig, J. Appl. Phys. **73**, 2724 (1993).
[13] D. E. Voss and S. A. Cohen, Rev. Sci. Instrum. **53**, 1696 (1982).
[14] K. Tominaga, M. Kume, T. Yuasa, and O. Tada, Jpn. J. Appl. Phys., Part 1 **24**, 35 (1985).
[15] M. A. Lieberman and A. J. Lichtenberg, *Principles of Plasma Discharges and Materials Processing* (Wiley, New York, 1994), p. 170.
[16] M. V. V. S. Rao, R. J. Van Brunt, and J. K. Olthoff, Phys. Rev. E **54**, 5641 (1996).
[17] A. V. Phelps, J. Appl. Phys. **76**, 747 (1994).
[18] A. V. Phelps, private communication (2007).
[19] S. H. Pullins, R. A. Dressler, R. Torrents, and D. Gerlich, Z. Phys. Chem. **214**, 1279 (2000).
[20] A. V. Phelps, C. H. Green, and J. P. Burke, Jr., J. Phys. B **33**, 2965 (2000).
[21] A. V. Phelps (unpublished).
[22] K. Kadota and Y. Kaneko, Jpn. J. Appl. Phys. **13**, 1554 (1974).
[23] A. V. Phelps and Z. Lj. Petrović, Plasma Sources Sci. Technol. **8**, R21 (1999).